# Simulation of ENSO-Related Surface Winds in the Tropical Pacific by an Atmospheric General Circulation Model Forced by Observed Sea Surface Temperatures

B. N. GOSWAMI

*Centre for Atmospheric Sciences, Indian Institute of Science, Bangalore, India*

V. KRISHNAMURTHY

*International Centre for Theoretical Physics and International Institute for Earth, Environmental and Marine Sciences and Technologies, Trieste, Italy*

N. H. SAJI

*Centre for Atmospheric Sciences, Indian Institute of Science, Bangalore, India*

(Manuscript received 19 April 1994, in final form 26 October 1994)

ABSTRACT

The authors present the simulation of the tropical Pacific surface wind variability by a low-resolution (R15 horizontal resolution and 18 vertical levels) version of the Center for Ocean–Land–Atmosphere Interactions, Maryland, general circulation model (GCM) when forced by observed global sea surface temperature. The authors have examined the monthly mean surface winds and precipitation simulated by the model that was integrated from January 1979 to March 1992. Analyses of the climatological annual cycle and interannual variability over the Pacific are presented. The annual means of the simulated zonal and meridional winds agree well with observations. The only appreciable difference is in the region of strong trade winds where the simulated zonal winds are about 15%–20% weaker than observed. The amplitude of the annual harmonics are weaker than observed over the intertropical convergence zone and the South Pacific convergence zone regions.

The amplitudes of the interannual variation of the simulated zonal and meridional winds are close to those of the observed variation. The first few dominant empirical orthogonal functions (EOF) of the simulated, as well as the observed, monthly mean winds are found to contain a large amount of high-frequency intraseasonal variations. While the statistical properties of the high-frequency modes, such as their amplitude and geographical locations, agree with observations, their detailed time evolution does not. When the data are subjected to a 5-month running-mean filter, the first two dominant EOFs of the simulated winds representing the low-frequency El Niño–Southern Oscillation fluctuations compare quite well with observations. However, the location of the center of the westerly anomalies associated with the warm episodes is simulated about 15° west of the observed locations. The model simulates well the progress of the westerly anomalies toward the eastern Pacific during the evolution of a warm event. The simulated equatorial wind anomalies are comparable in magnitude to the observed anomalies. An intercomparison of the simulation of the interannual variability by a few other GCMs with comparable resolution is also presented.

The success in simulation of the large-scale low-frequency part of the tropical surface winds by the atmospheric GCM seems to be related to the model's ability to simulate the large-scale low-frequency part of the precipitation. Good correspondence between the simulated precipitation and the highly reflective cloud anomalies is seen in the first two EOFs of the 5-month running means. Moreover, the strong correlation found between the simulated precipitation and the simulated winds in the first two principal components indicates the primary role of model precipitation in driving the surface winds. The surface winds simulated by a linear model forced by the GCM-simulated precipitation show good resemblance to the GCM-simulated winds in the equatorial region. This result supports the recent findings that the large-scale part of the tropical surface winds is primarily linear.

## 1. Introduction

Following the pioneering study by Lau (1985), who forced the Geophysical Fluid Dynamics Laboratory (GFDL) general circulation model (GCM) with observed tropical Pacific sea surface temperature (SST) for the period 1962–76, several other GCMs of different complexity have been integrated during the last decade with either observed near-global SST or tropical SST (Graham et al. 1989; Latif et al. 1990; Kitoh 1991; Kleeman et al. 1994). The primary motivation for most of these studies was to investigate the role of the slowly varying boundary condition (e.g., SST) in forcing the low-frequency variability in the Tropics (Charney and Shukla 1981; Shukla 1981). In recent years, these stud-

*Corresponding author address:* Dr. B. N. Goswami, Centre for Atmospheric Sciences, Indian Institute of Science, Bangalore 60 012, India.

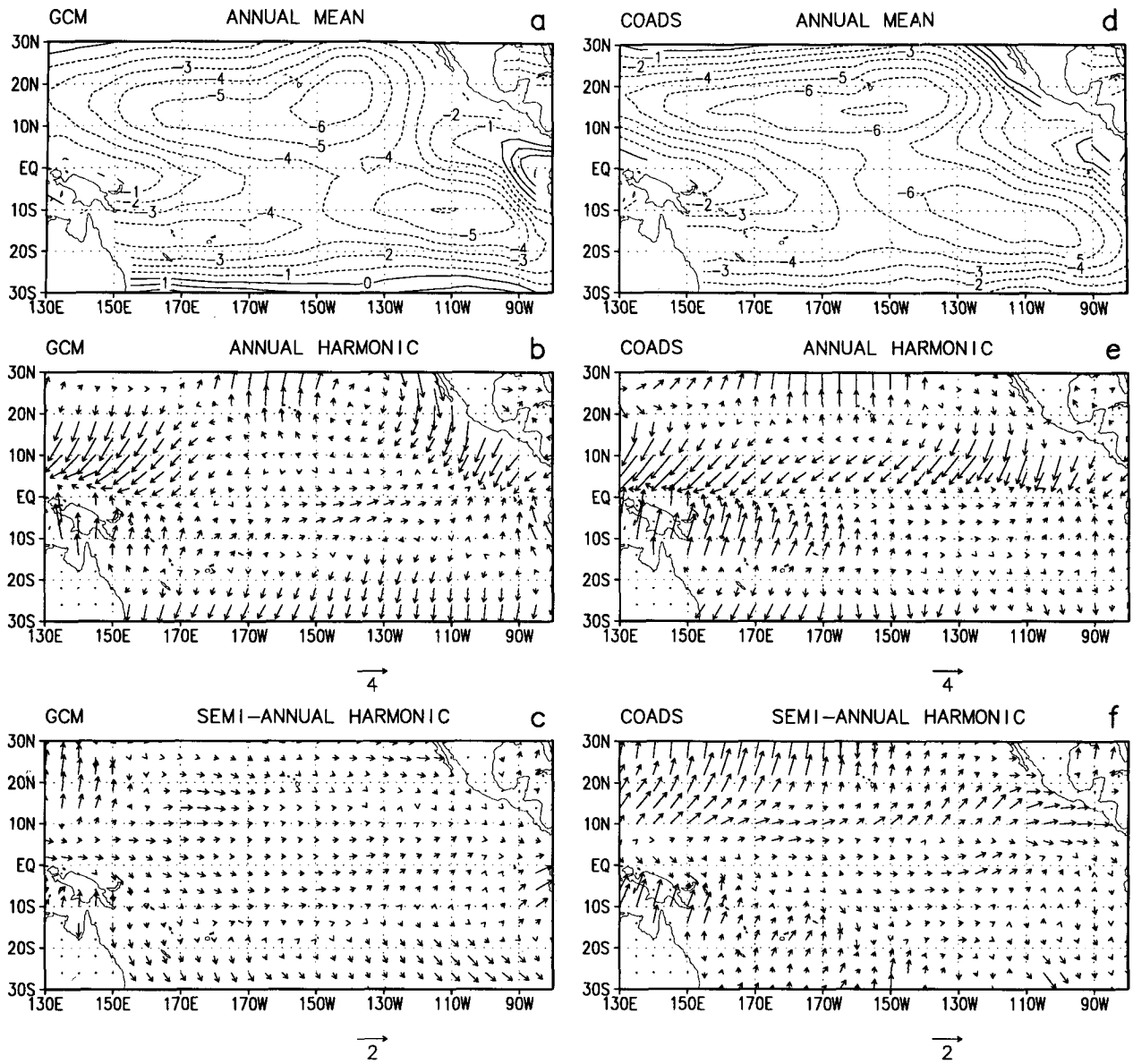


FIG. 1. Climatological mean zonal winds. (a) Annual mean, (b) annual harmonic, and (c) semiannual harmonic of the AGCM-simulated zonal wind, and (d) annual mean, (e) annual harmonic, and (f) semiannual harmonic of COADS zonal winds. The length of the arrow in both the harmonics represent the amplitude, while the direction of the arrow represent the phase. Pointing north means maximum occurs on 1 January, pointing east means maximum occurs on 1 April, and so on. For the second harmonic the phase represents time of the first maximum. The unit for the arrow is shown.

ies have assumed greater significance due to the pivotal role of the surface wind stress in coupled air–sea interactions leading to the El Niño–Southern Oscillation (ENSO) phenomenon. Coupled ocean–atmosphere models of varying complexity have been employed to simulate the ENSO phenomenon (Zebiak and Cane 1987; Neelin 1990; Schopf and Suarez 1988; Battisti 1988; Philander et al. 1992; Lau et al. 1992; Latif et al. 1993; Nagai et al. 1992; Neelin et al. 1992). Some of the simpler coupled models that specify the mean climate and predict only the departures from climatology (e.g., Zebiak and Cane 1987) tend to be more successful in simulating the interannual variability. On the other hand, more complex coupled GCMs tend to have difficulty in simulating realistic ENSO events (see Neelin et al. 1992). More recently, some complex coupled GCMs (Philander et al. 1992; Lau et al. 1992; Latif et al. 1993; Nagai et al. 1992) have been successful in simulating ENSO-like interannual variability. However, it is clear from these studies that the nature of the interannual variability simulated by these coupled GCMs are different from each other and seem

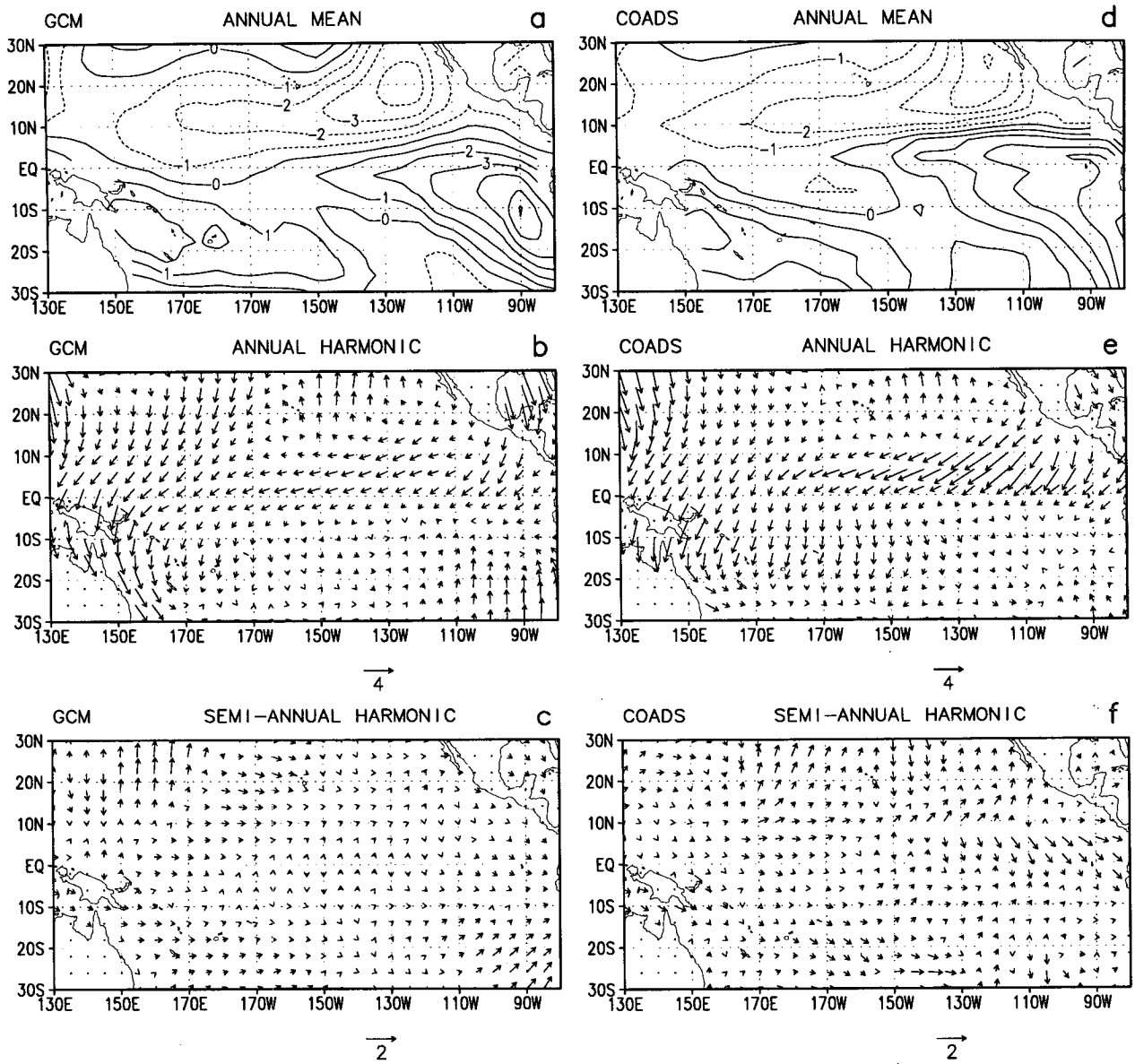


FIG. 2. Same as in Fig. 1 but for climatological mean meridional winds.

to depend critically on the resolution and parameterization of the physical processes. It is also recognized that the simulated interannual variability depends crucially on the strength and distribution of the coupling simulated by the model (Neelin et al. 1992). The coupling depends nonlinearly on the mean conditions such as the mean surface winds and the mean SST. Most GCMs have moderate systematic errors in simulating the mean climate. These systematic errors in the individual components in a coupled GCM can amplify due to unstable air–sea interactions and may result in climate drifts in coupled GCMs (Neelin et al. 1992). In this context, the ability of the atmospheric model to simulate the observed surface winds realistically when forced by observed SST is a prerequisite for using it in a coupled model.

The atmospheric component used in various coupled models range from the simple steady Gill model employed by Zebiak and Cane (1987) and Neelin (1990) to a low-resolution atmospheric GCM (AGCM) by Philander et al. (1992), Lau et al. (1992), and Latif et al. (1993) to a somewhat higher-resolution AGCM by Nagai et al. (1992). Most AGCMs produce appreciable systematic errors in simulating the climatological mean and variability of the tropical surface winds when forced by observed SST. The simple Gill-type models with atmospheric heating proportional to SST anomalies are known to produce far too strong easterlies in

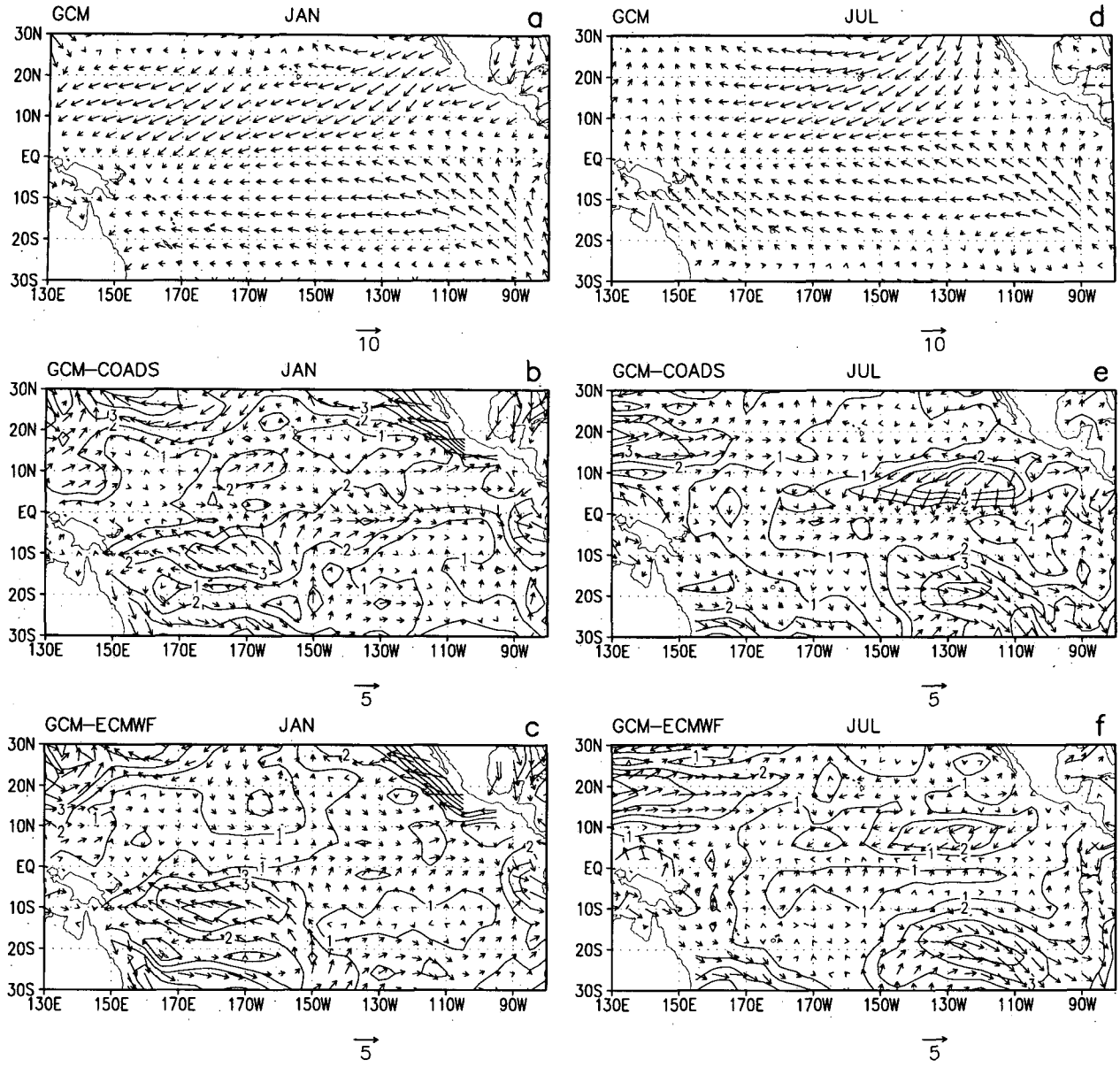


FIG. 3. AGCM-simulated climatological mean vector winds for January (a) and July (d). The differences between simulation and two observed climatologies (COADS and ECMWF analysis) are shown in (b) and (c) for January and in (e) and (f) for July. Solid lines represent isotachs of vector winds differences.

the eastern Pacific during warm phases of the ENSO (Zebiak 1986; Goswami and Shukla 1991). The low-resolution AGCMs also fail to correctly simulate the location of the maximum westerly anomaly and its asymmetry about the equator (Graham et al. 1989; Latif et al. 1990). AGCMs differ in the parameterizations of various physical processes, as well as in resolutions. Therefore, there is a need to assess the capability of an individual AGCM in simulating the annual cycle and interannual variability of the observed surface winds when forced by observed SST. With this objective in mind, we investigate the surface wind simulations by the R15 (rhomboidal 15) version of the Center for Ocean–Land–Atmosphere (COLA) Interaction AGCM when forced by observed SST.

The primary objective of the coupled models is to simulate the low-frequency interannual variability such as the ENSO. Some recent studies (Latif et al. 1990; Goswami and Shukla 1991) have shown that the large-scale part of the observed surface winds represented by the first two or three empirical orthogonal functions (EOFs) are sufficient to force the observed interannual variability in an ocean model. These studies indicate that the forcing associated with the small-scale high-

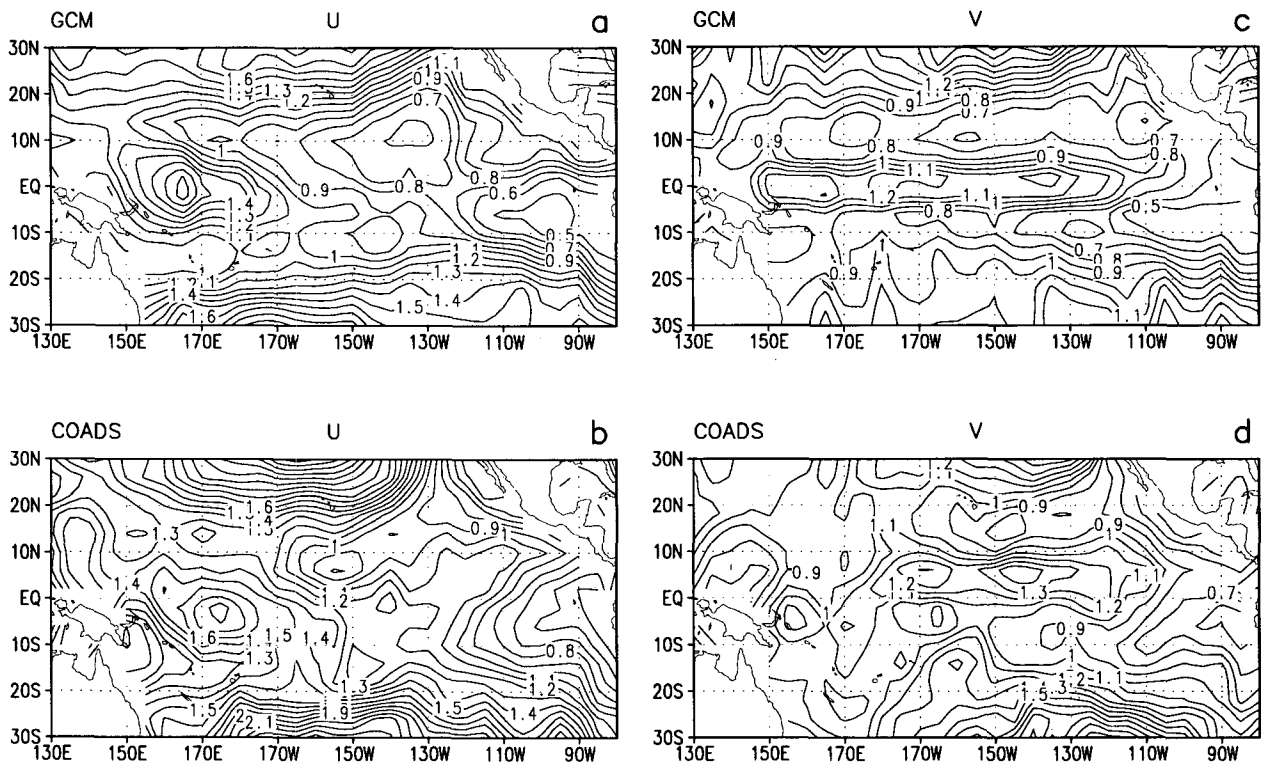


FIG. 4. Simulated and observed interannual standard deviation for zonal [(a), (b)] and meridional [(c), (d)] surface winds. The unit is meters per second.

frequency part of the surface winds is not essential in driving the low-frequency interannual variability in the ocean. In general, an AGCM simulates a broad range of space scales and timescales. Based on these studies, it may be concluded that an atmospheric model that simulates the large-scale part of the surface winds accurately may be a good choice for the atmospheric component in a coupled model even if it is not successful in simulating the small-scale high-frequency part of the surface winds well.

With this background, we analyze the model-simulated surface winds and compare them with observations with special emphasis on the annual cycle and large-scale low-frequency part of the variability. In section 2, we describe the model and the experiment. In section 3, we examine the simulated annual cycle of the surface winds and compare with observations. In section 4, we discuss the simulated interannual variability of the surface winds and compare it with observations. A summary and discussion is given in section 5.

## 2. The model and experiment

The model used in this study is a low-resolution version of the COLA AGCM. It is a spectral model with R15 horizontal resolution and 18 discrete vertical levels. The dynamics of the model are similar to the ones described by Sela (1980). The model employs primitive equations of motion with divergence, vorticity, virtual temperature, water vapor, and surface pressure as prognostic variables. Results from an earlier higher-resolution (R40) version of the model are described by Kinter et al. (1988). The model has a shallow convection scheme (Tiedke 1984), as well as a large-scale precipitation and cumulus convection scheme by Kuo (1965). The second-order closure model of Mellor and Yamada (1982) is used to parameterize the vertical diffusion at all levels. As discussed by Sato et al. (1989), the model includes the simple biosphere (SiB) model of Sellers et al. (1986).

The AGCM has been integrated using observed monthly mean SSTs from January 1979 through March 1992. The global SST used in this experiment is the blended SST (Reynolds 1988; Reynolds and Marsico 1993). The SST is obtained from an analysis of a blend of in situ data, AVHRR (Advanced Very High Resolution Radiometer) satellite data, and ice data. The integration was initiated from observed atmospheric data for 1 January 1979.

For comparison with observations we have used the surface winds from COADS (Comprehensive Ocean–Atmosphere Data Set) (Slutz et al. 1985) from January 1979 through December 1987. For the period between January 1988 to March 1992, we have used the

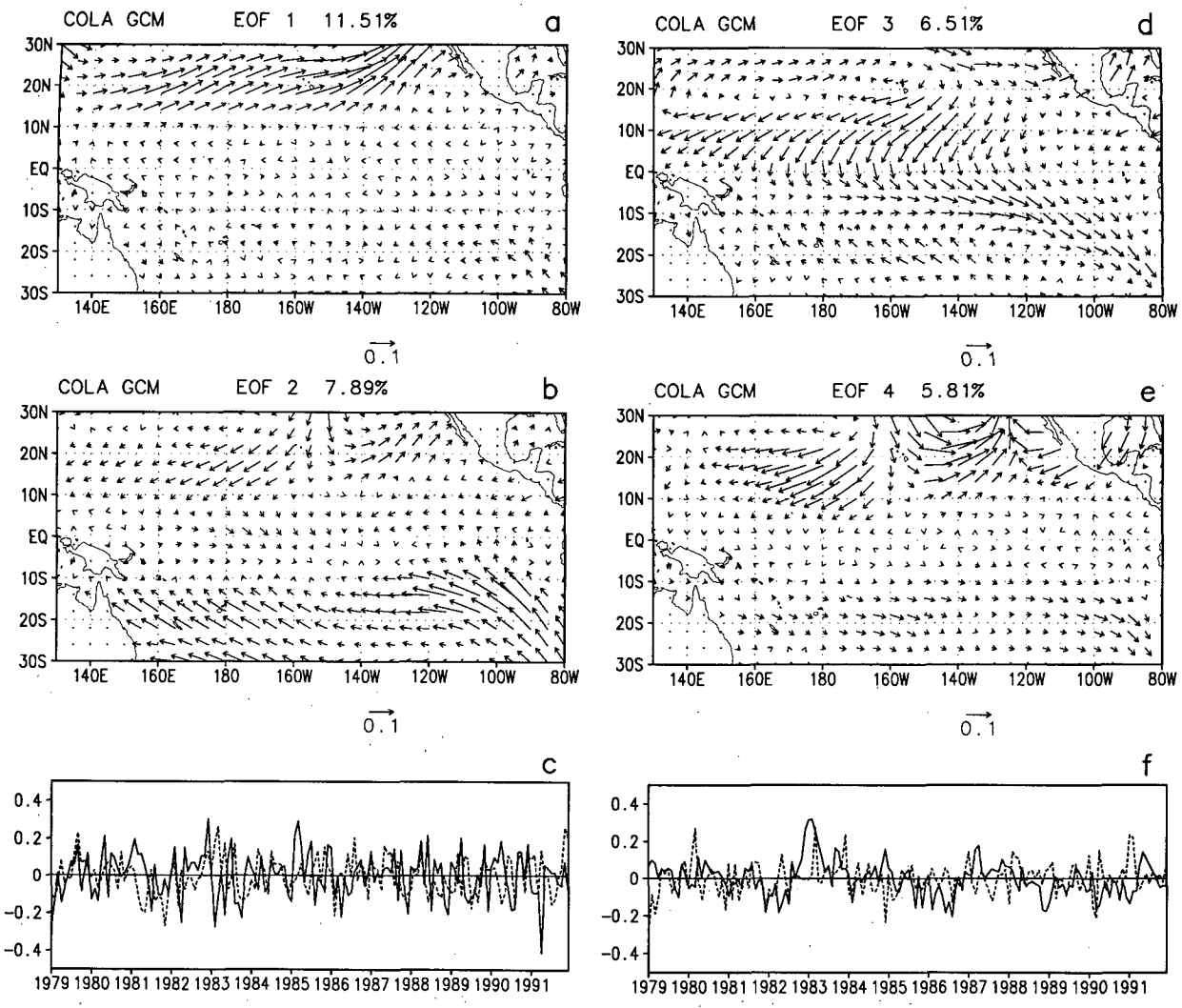


FIG. 5. First four EOFs and their principal components of the unfiltered monthly mean surface wind stresses simulated by the COLA GCM. The unit for the principal components is newtons per second.

ECMWF (European Centre for Medium-Range Weather Forecasts) analyses at 1000 mb. To compare large-scale structure of the simulated precipitation with observation, we have also used the highly reflective cloud (HRC) dataset between 1979 and 1987 (Garcia 1985).

## 3. The annual cycle

As mentioned earlier, the coupling between the atmosphere and the ocean depends sensitively on the mean climate of the individual components. Therefore, the correct simulation of the climatological annual cycle by the AGCM when forced by observed boundary conditions is equally important. In this section, we present the mean annual cycle simulated by the model and compare it with observations.

From the 13-yr model integration, climatological means for different calendar months were constructed for both zonal and meridonal components of the surface winds. The climatological monthly means were then Fourier-analyzed to extract the annual and semiannual harmonics at each grid point. Figures 1a–c show the annual mean, the annual harmonic, and the semiannual harmonic for the simulated zonal winds over the Pacific. The same fields for observations (COADS) are shown in Figs. 1d–f. The length of the arrow in the annual and semiannual harmonics represent the amplitude of the harmonic, while the direction represents the phase. The arrow pointing north represents the first maximum on 1 January, while the one pointing east represents the first maximum on 1 April and so on.

Comparison of the simulated annual mean zonal winds (Fig. 1a) with the observed (Fig. 1d) shows that the AGCM is quite successful in simulating the location of the strong trade winds between 10° and 20°N in the central Pacific and between 5° and 15°S in the eastern Pacific. It also properly simulated the weak easterlies

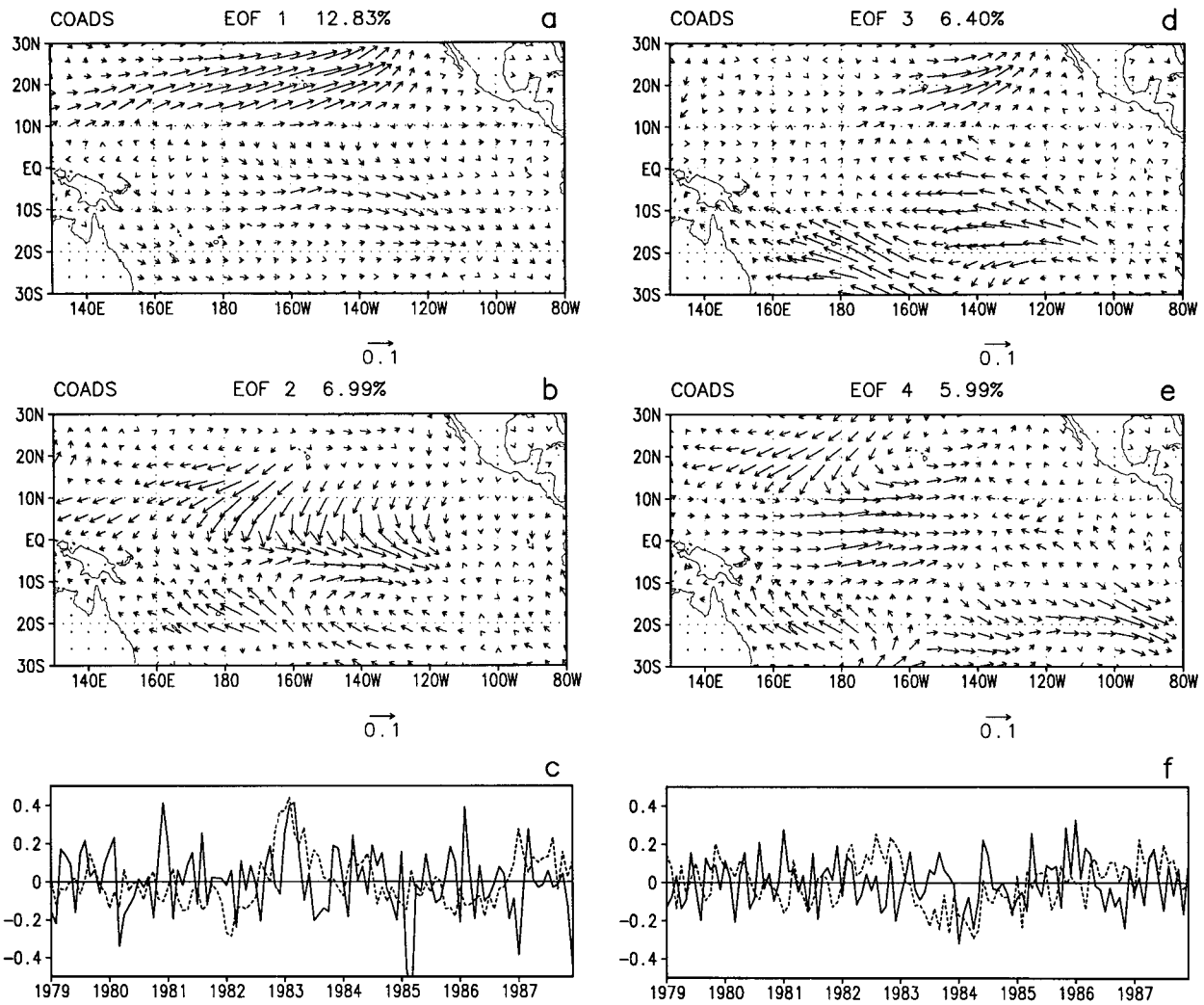


FIG. 6. Same as in Fig. 5 but for the COADS wind stresses.

in the convective zone of the South Pacific convergence zone (SPCZ) in the southwestern Pacific and the intertropical convergence zone (ITCZ) in the northeastern Pacific. However, the magnitude of the simulated strong trade winds in the southeastern Pacific is about 15%–20% weaker than observed.

The model also simulated the annual cycle reasonably well (Figs. 1b,e). The amplitude and the phase of the annual harmonic in the northwestern Pacific as well as in the south-central Pacific are well simulated by the model. In the north-central Pacific also, the amplitude is well simulated, but the maximum in the simulated zonal winds lag observations by about one month. There are two regions where the phase of the simulated annual cycle is correct but the amplitude is weaker than observed. They are in the 5°–15°N, 130°–100°W region in the eastern Pacific and in the 5°–15°S, 150°E–180° region. This systematic error of the model occurs over the two regions corresponding to the central regions of the ITCZ in the east and the SPCZ in the west Pacific. The amplitude of the semiannual harmonic in the observations is comparable to the annual harmonic only in the northwestern Pacific and in the westernmost part of southwestern Pacific (Figs. 1c, f). Elsewhere, the amplitude of the second harmonic is very small compared to that of the annual harmonic. The model also tends to produce the largest amplitude of the semiannual harmonic in the western Pacific (Fig. 1c). However, the model fails to simulate the large amplitude of the semiannual harmonic in the northwestern Pacific between 150°E and 160°W. In the regions where the amplitude of the semiannual harmonic is small, the simulated phases do not seem to correspond well with the observed phases.

Figure 2 shows the simulated (Figs. 2a–c) and observed (Figs. 2d–f) annual mean, annual harmonic, and semiannual harmonic of the meridional winds.

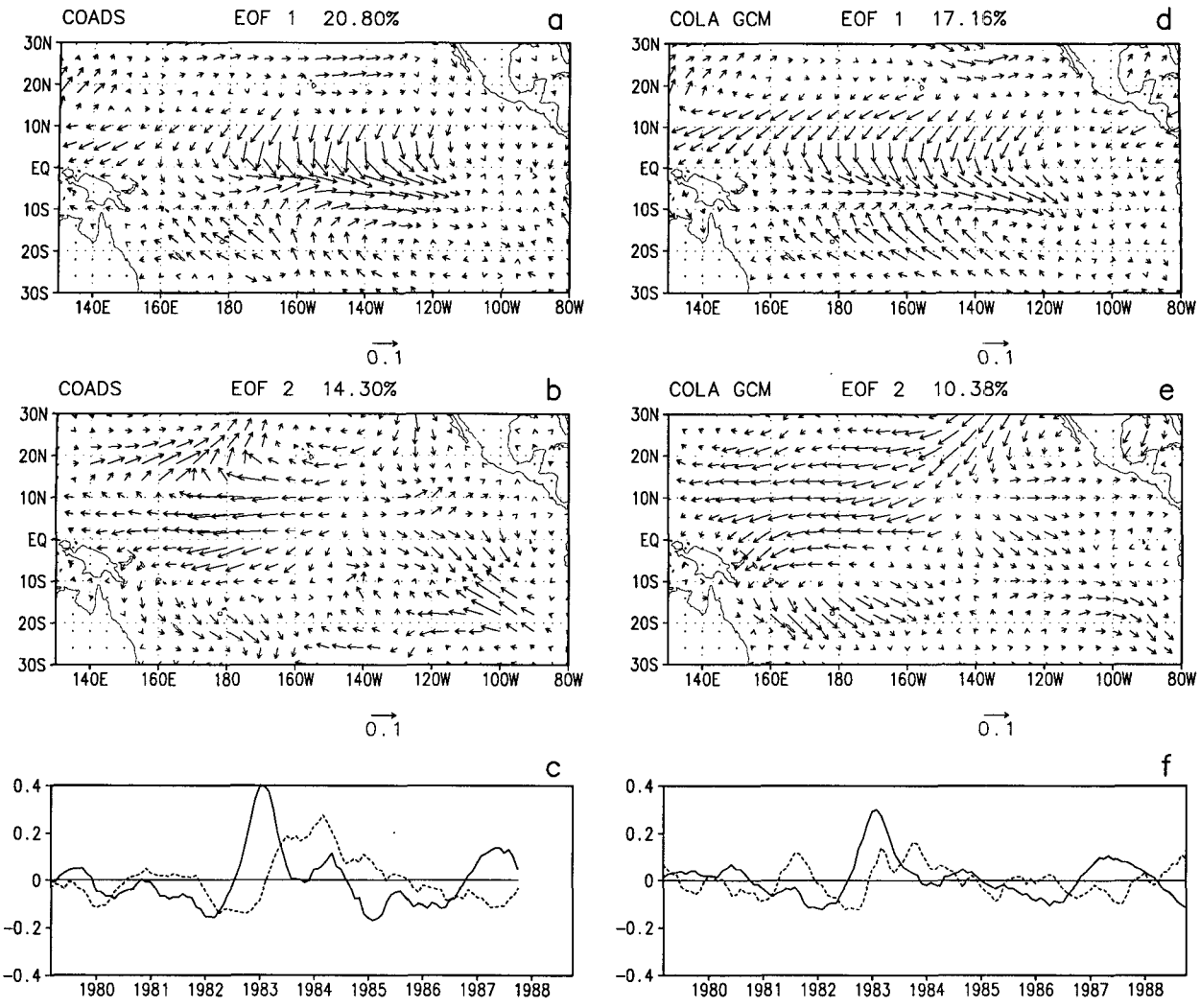


FIG. 7. Vector representation of the first two EOFs of AGCM-simulated filtered zonal (5-month running mean) ($U$) and meridonal ($V$) wind stresses and the corresponding principal components [(a), (b), (c)] together with the EOFs and PCs of corresponding fields of the observed winds [(d), (e), (f)]. The unit of the vector EOF loadings are shown. In (c) and (f), the solid line is PC1 and the dashed line is PC2.

Again, we note that the model simulated the location of the maximum northerlies and southerlies quite well. While the simulated mean zonal winds are somewhat weaker than observed, the simulated annual mean meridional winds are quite close to their counterparts in observations. Even the region of weak meridional winds running from southeastern Pacific to equatorial northwestern Pacific is well simulated by the model. The annual harmonic of the meridional winds is also well simulated in almost all locations except two small regions. In the ITCZ region north of the equator in the eastern Pacific, the phase of the annual cycle is correct but the amplitude is about one-half the observed amplitude. In the southeastern Pacific, the amplitude of the simulated annual harmonic is larger than that of the observed in the same region. The amplitude of the semiannual harmonic is again much smaller than that of the annual harmonic, both in observations and in model simulations. As with the zonal winds, the phases of the semiannual harmonic of the simulated meridional winds do not correspond well with those of the observed.

To supplement information about the simulated annual cycle provided in Figs. 1 and 2, the simulated vector winds for January and July are shown in Figs. 3a,d. They are compared with observed climatological vector winds for January and July derived from COADS, as well as ECMWF analyses. In Figs. 3b,c we show the vector difference between simulated winds for January and observed January winds from COADS and ECMWF analysis, respectively. The contours represent magnitude of the vector difference. Figures 3e, f contain similar differences for July winds. Although there are some differences between the climatologies derived from ECMWF analysis and COADS, the pattern of the differences between simulated winds and either of these climatologies is very similar. This indicates that

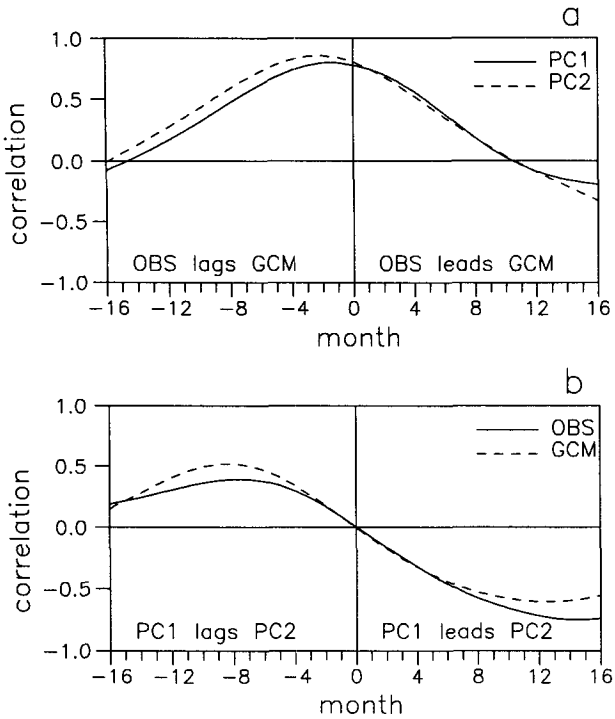


FIG. 8. (a) Lagged correlation between PC1 of observation and PC1 of AGCM simulation and between PC2 of observations and PC2 of AGCM simulations. (b) Lagged correlation between PC1 and PC2 for observed winds and AGCM simulated winds.

these differences are due to model deficiencies rather than to the differences in the climatologies. In summary, we note that major differences occur in the SPCZ region and in coastal central America. In the SPCZ region this difference is due to the fact that the center of the convergence zone located at around 10°S, 175°E is simulated by the AGCM about 15° to the west (around 160°E). This results in stronger than observed southeasterlies in the eastern side of the convergence zone.

In July, we note that the model performs well in simulating both the location and strength of the southeasterlies in the SPCZ region. In the ITCZ region in the eastern Pacific, the AGCM fails to simulate the strong southerlies around 130°W, resulting in the largest systematic errors in the equatorial region. The AGCM-simulated southeasterlies in the southeastern Pacific around 20°S, 120°W are also too weak compared to observations resulting in the northwesterly errors in this region.

Although the annual mean winds simulated by the AGCM correspond well with observations, we note some significant deficiency in simulating the annual cycle. The errors in simulations of January and July winds are manifestation of this deficiency in simulating the annual cycle. This is important in terms of air–sea interactions relevant to ENSO since observations indicate a certain phase locking of the ENSO with the annual cycle. Therefore, such errors in simulation of the annual cycle may lead to climate drift in a coupled model.

## 4. Interannual variability

### *a. Unfiltered variability*

Anomalies of zonal and meridional winds are obtained by subtracting the climatological mean for a given month from the individual monthly mean winds. To obtain an average measure of the interannual variations simulated by the model, standard deviation is calculated from the anomalies spanning the whole period of integration. Such standard deviations (SD) of the simulated zonal and meridional winds are shown in Fig. 4 and compared with similar SDs of the observed zonal and meridional winds. We note that the observed zonal winds have two low-variability regions corresponding to the regions of strongest trade winds in the northeastern Pacific and southeastern Pacific. Moreover, in the equatorial western Pacific, there is a region of high variability centered around 165°E. The model simulates the amplitude of the high variability quite well, but the location is shifted by about 10° to the west. Both centers of low variability in the eastern half of the Pacific are also well simulated. However, in these two regions, the amplitude of the interannual variability is much weaker (20%–30%) than observed. As in the case of the climatological mean winds, where we noted that the model simulations of the meridional component is better compared to the simulations of the zonal component, the amplitude of interannual variability of the meridional winds also appears to be better simulated than that of the zonal component. The SD of the simulated meridional winds is close to or slightly larger than that of the observed winds in almost all the locations. The only notable discrepancy is in the simulation of the location of the largest SD in the central and eastern Pacific where the model simulates the largest variability over the equator, while in the observations the largest variability tend to occur around 5°N.

The simulated as well as the observed surface winds exhibit considerable high-frequency month-to-month variability. If the high-frequency variability in the surface winds simulated by our AGCM is too large compared to observations, it may adversely affect the simulation of the low-frequency variability by an OGCM. To get a better idea about the amplitude and structure of this high-frequency component, we carried out EOF analysis of the unfilitered monthly mean simulated and COADS winds. Figure 5 shows the first four EOFs of the simulated winds and their corresponding principal components (PCs). Similarly, Fig. 6 shows the first four EOFs and their PCs of the COADS winds. We note that the total variance explained by the first four EOFs of the simulated winds (30.94% of total) compares well with that of the COADS winds (31.92% of total). The percentage of variance explained by indi-

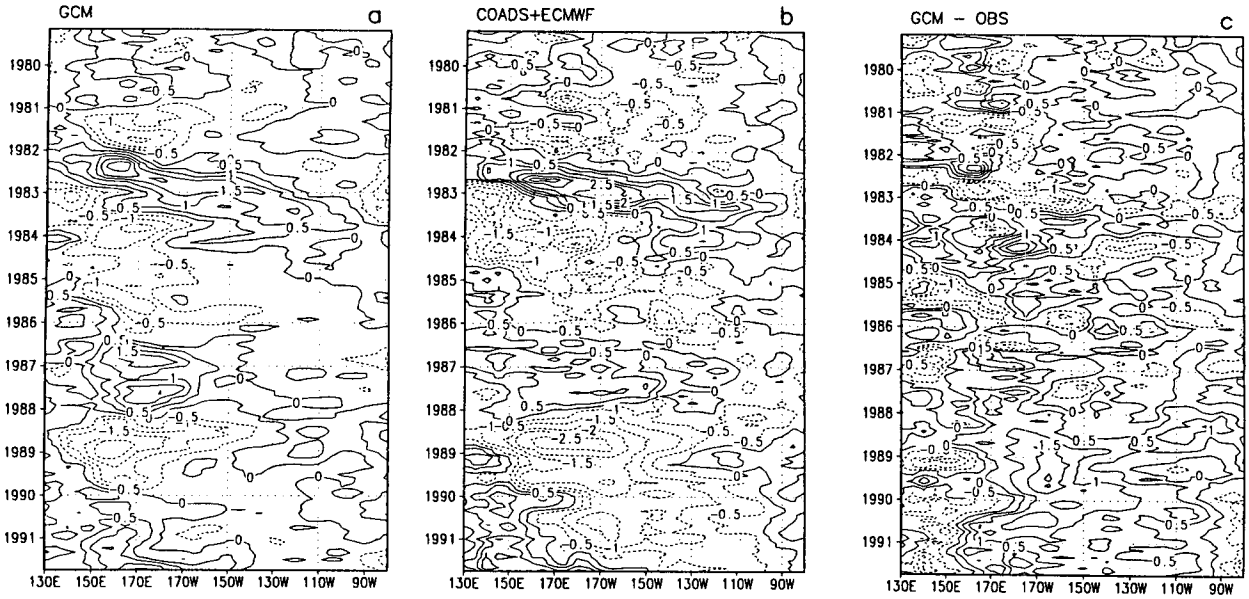


FIG. 9. Simulated and observed filtered (5-month running mean) zonal winds averaged between 6°S and 6°N across the equatorial Pacific basin as a function of time. In (b), up to December 1987, COADS data are used. From January 1988 onward, data from ECMWF analysis are used. Negative contours are dashed lines. Contour interval is 0.5 m $s^{-1}$. (c) Differences between simulated and observed winds.

vidual EOFs of the simulated winds are also comparable to those of the corresponding EOFs of the COADS winds. One interesting observation is that the first EOF of both the simulated and COADS winds is dominated by off-equatorial patterns. This appears to be associated with extratropical high-frequency variability. It appears that a part of the observed EOF1 pattern is simulated by the model as a part of the EOF2. Similarly, a part of the observed EOF2 is simulated by the model as a part of EOF1. This is because a certain high-frequency component is simulated by the model with higher amplitudes than that in the COADS winds, while that of another high-frequency component is simulated by the model with a lower amplitude than observed. In contrast to EOF1 and EOF2, the EOF3 for the simulated, as well as the COADS, winds is dominated by an equatorial pattern. An examination of the PCs clearly indicates that all the EOFs are associated with considerable high-frequency component both for the simulated and the COADS winds. Spectrum analysis (not shown) of the PCs show that the amplitude of the high-frequency component in the simulated wind is close to the amplitude of the high-frequency component of the COADS. We also note that the correlation between the corresponding PCs of the simulated and COADS wind is quite poor. Therefore, it is not fair to compare the first two EOFs of the simulated winds with corresponding EOFs of the COADS winds. The sum of the first two EOFs of the simulated winds correspond reasonably well with the sum of the first two EOFs of the COADS winds. The lack of correspondence in the temporal evolution of these patterns is expected since part of the high-frequency variability is due to internal dynamics and hence sensitive to initial conditions. The statistical properties of the high-frequency oscillation, such as their amplitude and combined pattern, seem to be reasonably well simulated by the model.

### *b. The low-frequency variability*

As the simulation of the large-scale low-frequency part of the surface winds by the AGCM is crucial for interannual variability studies, we subject the simulated and the observed surface winds to a 5-month running-mean filter. The EOFs of the filtered wind stresses are constructed, and we show in Fig. 7 the first two EOFs of the simulated surface wind stresses and compare them with those of the observed wind stresses. As in Figs. 5 and 6, the EOFs are constructed using the zonal and meridional wind anomalies as a combined variable, and the wind vectors are then constructed from the zonal and meridional components of the eigenfunctions. Both the pattern and the amount of variance explained by the first EOF of the simulated winds agree well with those of the COADS winds. While the amplitude of the simulated 1982–83 winds associated with the warm episode is weaker than observed by about 20%, those corresponding to the 1987–88 event are simulated quite well. The mean convergence zone is simulated around 5°S as in observations. The divergence zone around 20°N, 130°W is also well simulated by the model. The only discrepancy between the simulation and the observations is in the location of the largest westerly anomalies. While in the observations it occurs around 160°W, the model simulates it around 170°W. The second EOF explains relatively smaller

amount of variance in the model simulations as compared to that in the observation. The pattern of the simulated second EOF agrees well with the second EOF of observations, except in the North Pacific around the date line.

The PCs corresponding to the first two EOFs are also shown in Fig. 7. Keeping in mind the patterns of EOF1 and EOF2, the phase difference between PC1 and PC2 during 1982–83 clearly shows that the AGCM is able to simulate the observed eastward migration of the westerly wind anomalies from western Pacific to eastern Pacific during the evolution of the strong warm episodes. We note that during the 1987–88 episode, there was no prominent eastward propagation of the westerly anomalies, and this feature is also simulated well by the model. It is also clear from the PCs of the first and second EOFs that both these patterns are related to the low-frequency ENSO mode. The higher EOFs contain smaller horizontal scales. The agreement between the simulated and observed patterns corresponding to higher EOFs is poor.

Figure 8a shows the lagged correlations between the observed and simulated principal components. It shows that both PC1 and PC2 are equally well simulated at zero lag. Both of them are best simulated when observations lag AGCM simulations by about three months. Noting the high correlation ($\sim$0.88) between observed and simulated PC1 and PC2 of the filtered winds at zero lag, we can conclude that the model is able to simulate the low-frequency part of the variability both in temporal, as well as in spatial, patterns. Figure 8b shows the lagged correlations between PC1 and PC2 for both observations and simulations. We see that PC1 and PC2 are positively correlated when PC1 lags PC2 and negatively correlated when PC1 leads PC2. The model simulates this feature quite well. In conjunction with the spatial patterns of these EOFs shown in Fig. 7, this feature means an eastward propagation of the zonal wind stress anomalies during a warm episode. The simulated winds show that the model simulates this feature successfully. This is a quantitative support of the qualitative statements we made while discussing Fig. 7.

The EOFs discussed in Figs. 7 and 8 represent the large-scale patterns. Tropical air–sea interactions are particularly sensitive to the winds near the equator. To examine the simulations of the equatorial winds more closely, we show in Fig. 9 time–longitude sections of observed and simulated zonal winds averaged between 6°S and 6°N and filtered using a 5-month running mean. It is seen that the model successfully simulates the major features of the equatorial zonal wind variability both in amplitude and in their temporal evolution. For example, the easterly anomalies in 1981 confined to the west of 170°W are well simulated. So are the westerly wind anomalies during 1982–83 and their eastward migration. The magnitude of the simulated westerly anomalies closely correspond to observations. The easterly anomalies starting in the westernmost part of Pacific, stretching up to 1986 in the central Pacific, are also well simulated by the AGCM. The model also simulates the westerlies in the western and central Pacific during 1986–87 and easterlies during 1988–89 quite well. Closer scrutiny, however, reveals that there are some systematic errors in the simulated equatorial winds. Figure 9c shows the difference between the filtered GCM and observed winds averaged over 6°S–6°N. One striking feature of this difference field is that it is characterized by small zonal-scale errors. This means that even though the model simulates the large-scale part of the low-frequency oscillations represented by EOF1 and EOF2, there are some low-frequency small-scale oscillations (represented by the higher EOFs of the filtered winds) that the model is unable to simulate well. Even for the large-scale patterns, the model tends to simulate the pattern about 3 months before observations (Fig. 8a). This results in some systematic errors. Moreover, the model tends to underestimate the easterly anomalies over the central Pacific. This results in the positive difference between 1988–91 and 1984–86. These systematic errors may play an important role in air–sea interactions in a coupled model.

### c. *Comparison with simulations by some other GCMs*

While detailed intercomparison between a large number of models is outside the scope of this study, to put the simulations of this model in perspective we have made an attempt to compare the simulation of surface winds by the COLA model with simulations of the same by a few other models with similar resolutions. For this purpose, we were able to obtain simulated surface wind stresses by three other models from the AMIP (Atmospheric Model Intercomparison Project; Gates 1992). They are (a) Meteorological Research Institute, Japan (MRI GCM), with 4° latitude by 5° longitude horizontal resolution and 15 hybrid levels in the vertical; (b) Goddard Laboratory for Atmospheres (GLA GCM) with 4° latitude by 5° longitude horizontal resolution and 17 sigma levels in the vertical; and (c) State University of New York, Albany, model (SUNYA GCM). This is based on NCAR CCM1 with rhomboidal 15 horizontal resolution and 12 sigma levels in the vertical. All the models were run with observed global SST from January 1979 to December 1988.

In Fig. 10 we compare the simulation of the low-frequency component of the surface winds stress by the three different models. Here we show the first two EOFs and the accompanying principal components of the 5-month running-mean stresses. We can compare these patterns and their amplitudes with those from COADS and COLA GCM in Fig. 7. We note that these two patterns do represent the low-frequency variability associated with the ENSO in all the models. However, the dominant pattern (EOF1) has some significant differences. The MRI GCM patterns have too zonal winds

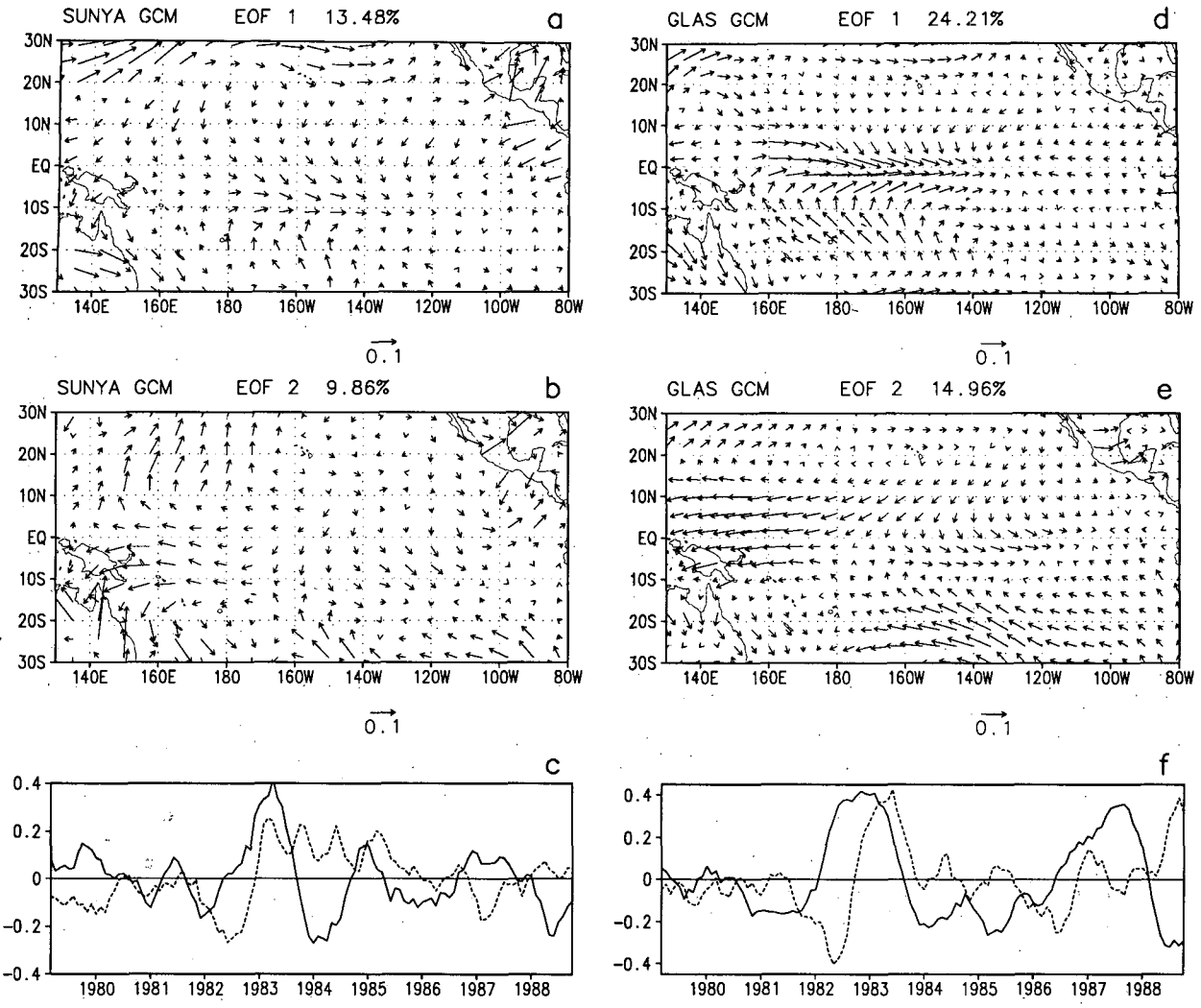


FIG. 10. The first two EOFs and their principal components of filtered (5-month running mean) vector wind stresses simulated by three different models. Convention of plotting is same as in Fig. 7.

in the central Pacific, and the westerlies do not extend up to 110°W and do not have the tongue toward the Southern Hemisphere. As a result, it has too weak convergence in the eastern Pacific associated with this pattern. The GLA GCM pattern also has westerlies terminating at about 130°W and does not have the tongue extending to the Southern Hemisphere. The COLA GCM, however, does a much better job of capturing the dominant pattern. The amplitude of the EOFs of the COLA GCM, on the other hand, is weaker than observed during 1982–83. The amplitude of the other three models during 1982–83 are comparable to that observed. In Table 1 we give the correlations between observed and simulated principal components of the first two dominant EOFs. We note that the correlations between PCs of COADS winds and COLA GCM-simulated winds are among the highest. We argue that not only the amplitude but also the convergences and divergences associated with the dominant patterns are important for large-scale air–sea interactions. For example, too weak convergence simulated by a GCM in its EOF1 may lead to weaker equatorial upwelling, weaker cold tongue, and weaker horizontal temperature gradient in the ocean model and to climate drift in a coupled model.

As equatorial winds are of special importance in the tropical air–sea interactions, we also compare zonal and meridonal stresses averaged over 5°S–5°N, 180°–140°W in Figs. 11 and 12. It is clear from Fig. 11 that all the models simulate the general tendency of the interannual variation of the zonal winds. However, there are considerable variations from model to model. If we concentrate on 1982–83 event, SUNYA tends to overestimate the zonal stress while COLA tends to underestimate it. MRI and GLA simulate approximately the right amplitude. The stress in different models, however, are calculated using bulk formulas where the value of the drag coefficient is not the same. Therefore,

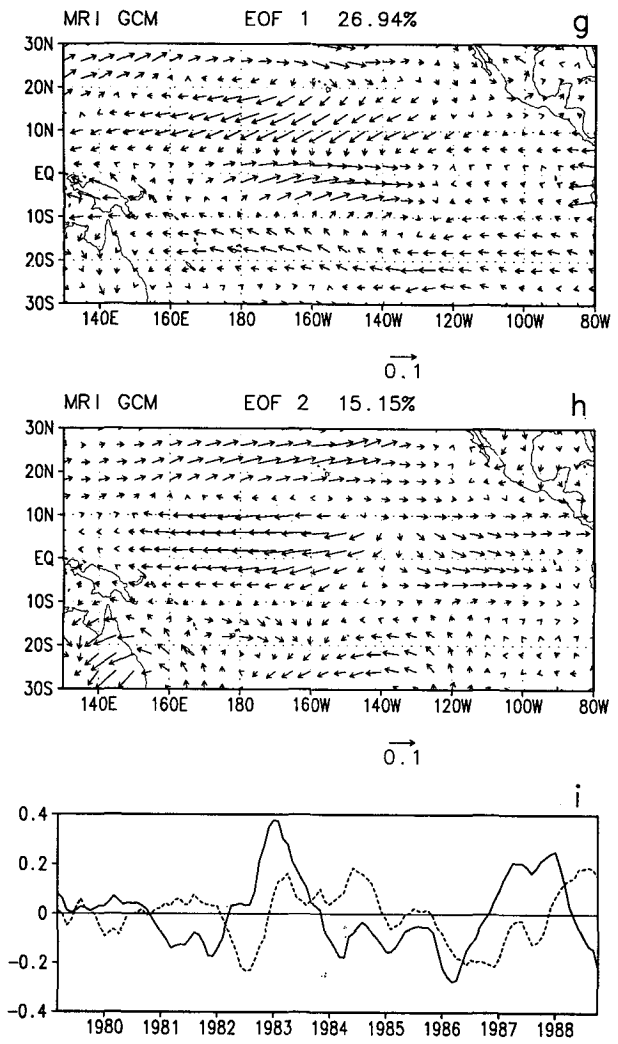


FIG. 10. (*Continued*)

it is not fair to compare the actual magnitude of the stress of the different models. We calculated the stress of the COLA model and the COADS winds using the same drag coefficient. Therefore, the weak simulation of the 1982–83 event by the COLA model is real. For the meridional stress (Fig. 12), the SUNYA model again tends to overestimate the amplitude of the interannual variations, while MRI totally fails to simulate the interannual variations in this region. This is consistent with the too zonal structure of the leading EOFs (Fig. 10) of MRI stress. Both GLA and COLA simulate the observed interannual variation of the meridional stress in this region well.

We want to emphasize at this point that this is a rather limited intercomparison. The objective here is to give an idea about the spread in simulating the interannual variability by a class of models with similar resolutions. We are currently in the process of getting results of about 20 AGCMs for making a detailed intercomparison of surface winds simulated by the GCMs.

## 5. Summary and discussions

To summarize, we note that the relatively low-resolution AGCM is successful in simulating the annual cycle and the interannual variability reasonably well. The locations of the trade winds, the ITCZ, and the SPCZ are all well simulated. The strength of the simulated climatological mean zonal winds in the strong trade wind belt is about 15%–20% weaker than those observed. The amplitude of the annual cycle of the GCM-simulated surface winds is close that of COADS winds everywhere except over the ITCZ and SPCZ regions. In these two regions, the simulated amplitude is much weaker than observed. The amplitude of the simulated interannual variability is comparable to the amplitude of observed interannual variability. The AGCM simulates the statistical properties of the high-frequency modes, such as their amplitude and geographical location, reasonably well. However, understandably, it does not simulate their temporal evolution well. The AGCM simulates the low-frequency large-scale component of the surface winds variability well both in spatial patterns and in their temporal evolution. The agreement between the simulation and observations in the case of first two EOFs of the filtered (5-month running mean) winds is noteworthy. The model also simulates the equatorial westerly (easterly) anomalies and their eastward migration during warm (cold) phases of the 1982–83 ENSO well.

The successful simulation of the large-scale part of the surface winds seems to be related to the successful simulation of the large-scale part of the precipitation by the AGCM. The first two EOFs of the filtered model-simulated precipitation field are shown in Fig. 13 along with PCs. Comparing the PCs of the model precipitation with those for the first two EOFs of the model surface winds (Fig. 7), it is clear that there exists a strong correspondence between the precipitation PCs and the surface wind PCs. The correlation between the first two PCs is 0.94, while that between the second two PCs is −0.89. This indicates that the large-scale part of the simulated winds is driven primarily by the large-scale part of the model precipitation. In an attempt to compare the model's simulation of the large-scale part of the precipitation with observations, we show in Fig. 14 the first two EOFs of the highly reflective cloud (HRC) index. The agreement between the first two EOFs of the model precipitation with those of the HRC anomalies is quite remarkable. HRC rep-

TABLE 1. Correlation coefficients between principal components of the first two EOFs of the observed 5-month running-mean COADS winds and those simulated by the four models.

| COADS | PC1 | PC2 |
|---|---|---|
| COLA | 0.88 | 0.61 |
| SUNYA | 0.54 | 0.72 |
| GLA | 0.61 | 0.40 |
| MRI | 0.80 | 0.67 |

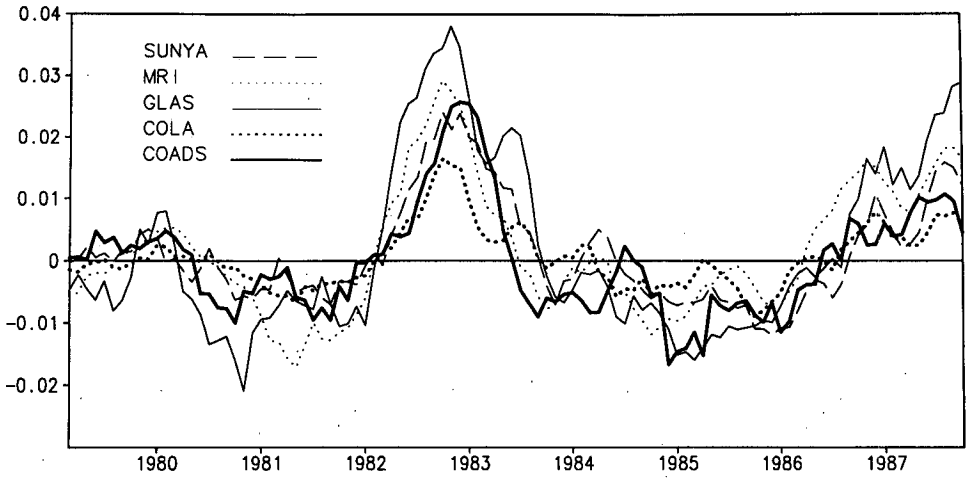


FIG. 11. Comparison of zonal stress (N $m^{-2}$) averaged between 5°S and 5°N, 180° and 140°W for four models with that from COADS.

resents primarily deep convective clouds. Thus, the large-scale organized part of precipitation seems to come from deep convective clouds, and the AGCM is quite successful in simulating them.

To get a better idea about the model's simulation of the precipitation in the equatorial region, the precipitation anomalies averaged between 6°S and 6°N along the tropical Pacific is shown in Fig. 15 as a function of time and compared to a corresponding time–longitude section of the HRC anomalies. We see that the model simulates the propagation of positive precipitation anomalies from the western to the eastern Pacific during warm episodes of 1982–83 and 1987–88. It also shows increased precipitation in the eastern Pacific and decreased precipitation in the western Pacific in the mature phase of the warm episodes (e.g., end of 1982 and beginning of 1983, end of 1987 and beginning of 1988). The model also simulates the decreased precipitation in the central Pacific during cold phases of ENSO, such as 1984 and 1988. All these features correspond well with observations as shown by the HRC anomalies. The HRC data was also available only up to December 1987.

Thus, it is clear from Figs. 7, 13, 14, and 15 that the successful simulation of the large-scale part of the zonal winds by the AGCM is a result of the AGCM's ability to simulate the large-scale part of the precipitation field well. Some recent studies (Neelin 1988; Zebiak 1990) indicate that the nonlinearities are of secondary importance in maintaining the large-scale part of the tropical surface winds. Zebiak (1990) also shows that a linear model may be able to simulate the tropical surface winds quite well if it can simulate the convective heating field well. As the convective heating results from various nonlinear thermodynamic and dynamic processes, the linear models usually have difficulty in parameter-

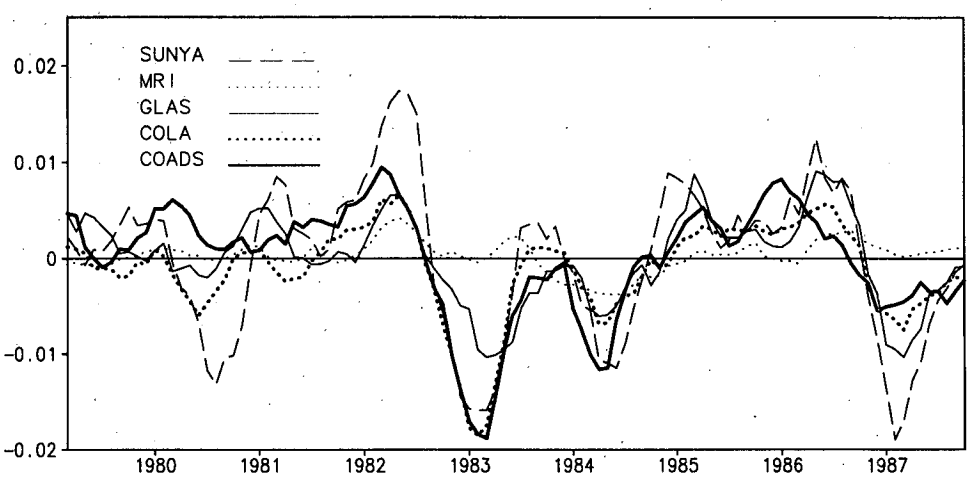


FIG. 12. Same as in Fig. 11 but for meridional stress.

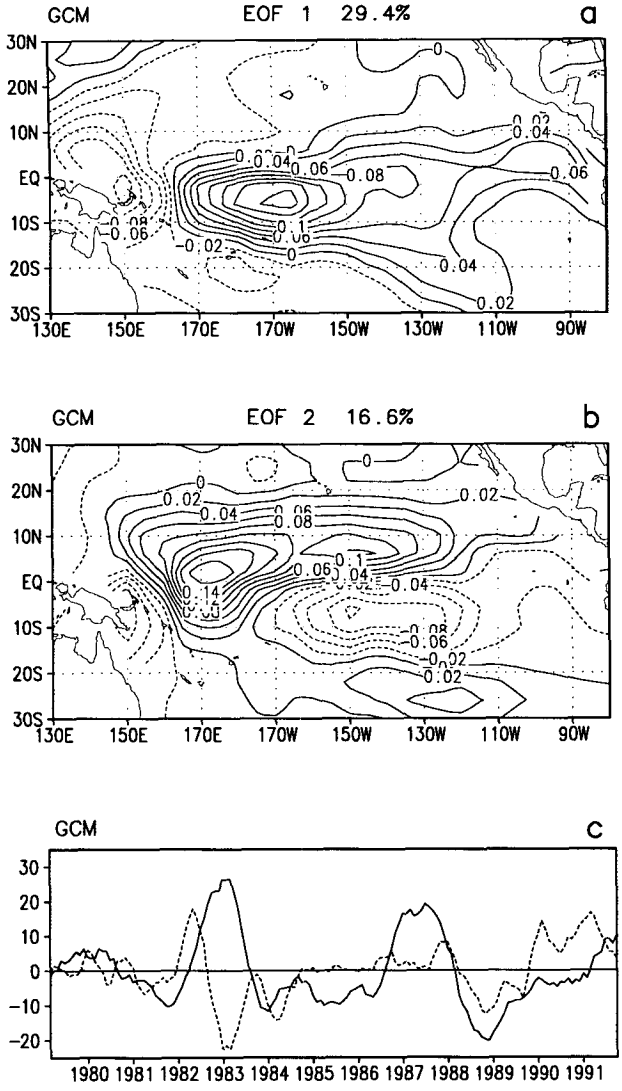


FIG. 13. The first two EOFs and their corresponding PCs of the filtered (5-month running mean) AGCM-simulated precipitation anomalies. The solid line in (c) is PC1 and the dashed line is PC2.

izing the heating field well. However, if the heating field is externally prescribed, a linear model may be expected to simulate the tropical winds quite well. To derive further insight regarding the maintenance of the tropical surface winds simulated by the AGCM, we ask the following question. How much of the AGCM-simulated winds may arise as a result of linear dynamics forced by the AGCM-simulated precipitation anomalies? For this purpose, we constructed a linear model described by

$$u_t - fv + \phi_x + \epsilon u = 0$$

$$v_t - fu + \phi_y + \epsilon v = 0$$

$$\phi_t + C^2(u_x + v_y) + \epsilon\phi = -Q - bT_s. \qquad (1)$$

This model takes into account the forcing associated with deep convection, represented by $Q$, as well as the forcing associated with the surface temperature gradients (Lindzen and Nigam 1987) represented by the term $bT_s$, where $T_s$ is the SST. Since Lindzen and Nigam's boundary layer equations can be reduced to Gill model equations using a suitable transformation (Neelin 1989), they can be combined to give (1) (Eltahir and Bras 1993). In (1), $u, v$ may be interpreted as perturbations in horizontal mass flux in the boundary layer, and $\epsilon$ is Raleigh friction parameter. The forcing function associated with deep convection is parameterized as

$$Q = \alpha P, \qquad (2)$$

where $P$ is the precipitation in millimeters per day. The dimensional values of the parameters used are $\alpha = 3.0$ kg s$^{-3}$ mm$^{-1}$ day, $\epsilon = (1 \text{ day})^{-1}$, $C = 17.45$ m s$^{-1}$, and

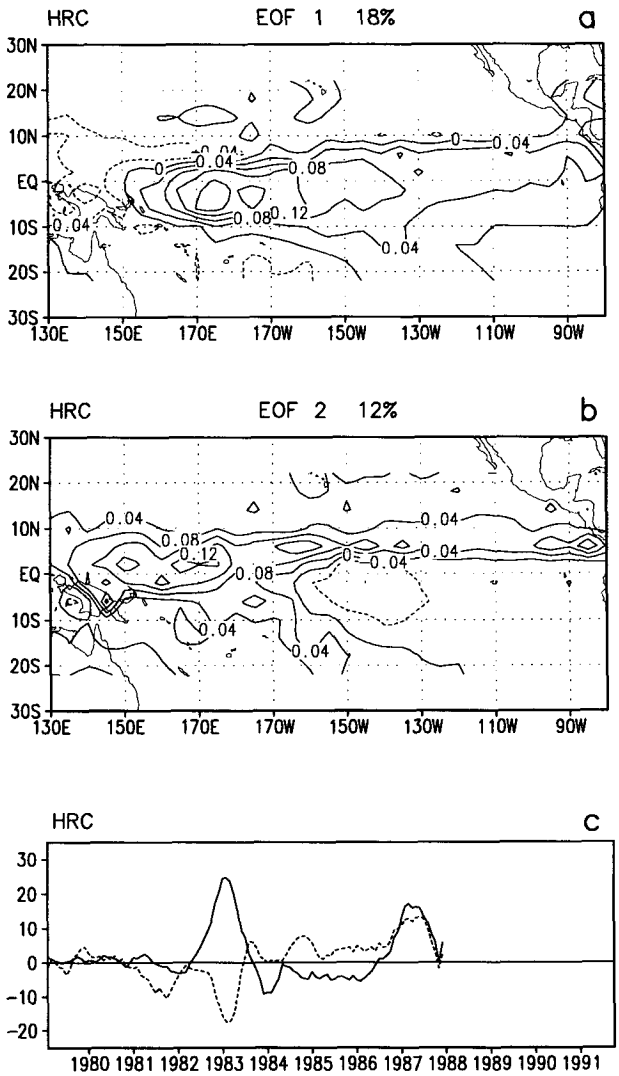


FIG. 14. The two EOFs and their corresponding PCs of the filtered (5-month running mean) HRC anomalies. The solid line in (c) is PC1 and the dashed line is PC2.

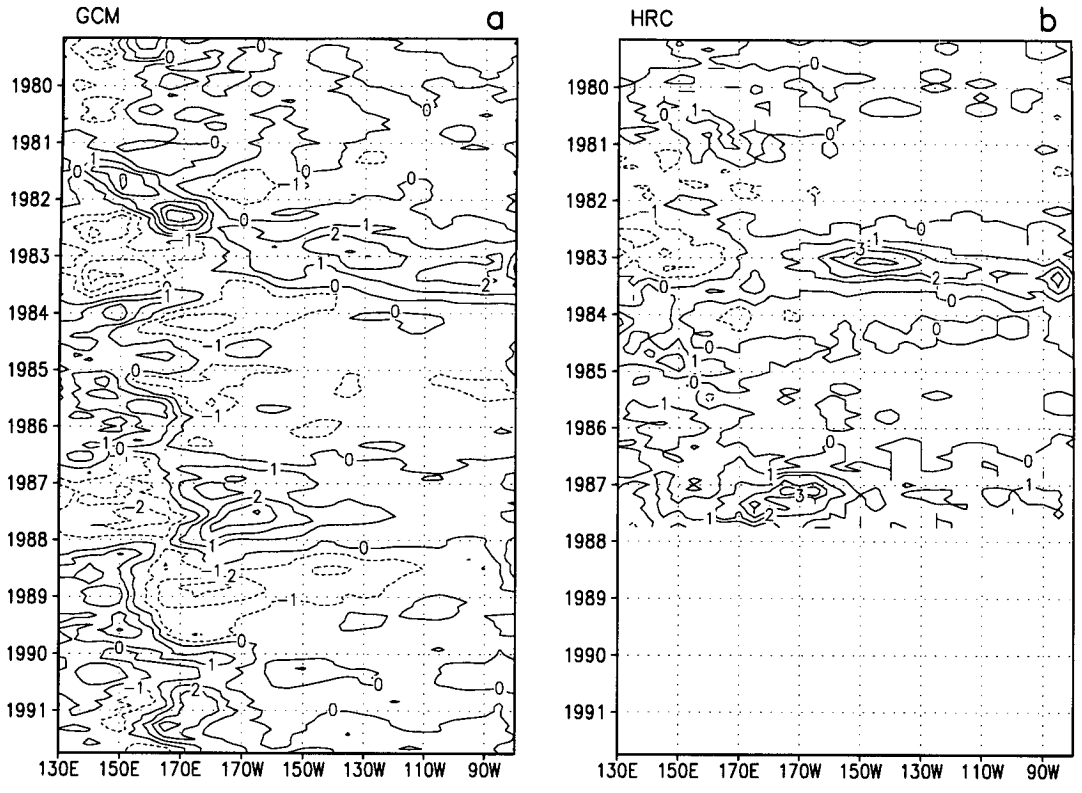


FIG. 15. Filtered (5-month running mean) AGCM-simulated precipitation anomalies (a) and HRC anomalies (b) averaged between 6°S and 6°N along the equatorial Pacific basin with time.

$b = 1.808$ kg s$^{-3}$. Using the precipitation anomalies for each month obtained from the AGCM and the corresponding SSTs, the steady solution corresponding to each month from January 1979 to March 1992 were obtained by numerically integrating (1). As with the AGCM data, the surface winds obtained from this linear model were then filtered into 5-month running means. The filtered winds were subjected to EOF analysis. The first two EOFs and their principal components of the surface winds simulated by the linear model are shown in Fig. 16. It is interesting to note that there is good correspondence between the AGCM EOFs (Fig. 7) and the linear model EOFs within the equatorial domain, approximately between 15°N and 15°S. Some discrepancies between the patterns are seen only near northern and southern boundaries of our analysis domain. In the first EOF, maximum convergence taking place around 5°S, 170°W is well simulated by the linear model. Similarly, larger easterlies in the northeastern Pacific and very weak easterlies in the southeastern Pacific are also well simulated. Several features of the second EOF are also well simulated. To further examine the simulation of the equatorial winds by the linear model, linear-model–simulated zonal wind averaged between 6°S and 6°N is shown as a function of time in Fig. 17. Comparing this with Fig. 9, we note that west of the date line the linear model simulated the AGCM zonal winds quite well. For example, the westerly maximum around 160°E in early 1982, the easterlies during late 1983 and early 1984, the westerlies in 1987, the easterlies in 1988–89, and the westerlies in 1991 are all well simulated. Between the date line and 160°W, however, there are small differences between the AGCM-simulated zonal winds and the ones simulated by the linear model. For example, the weak easterlies east of the date line during 1984–85 simulated by the AGCM are replaced by weak westerlies (<0.5 m s$^{-1}$) in the linear model's simulations. Similarly, the easterlies during 1988–89 do not extend beyond the date line in the linear model as it does in the AGCM simulations. This discrepancy may be partly due to the nonlinear effects. In summary, a linear model forced with AGCM precipitation can successfully simulate the major features of equatorial winds. While the nonlinearity does not seem to be of great importance in driving the equatorial winds, they seem to be important in driving the off-equatorial subtropical winds.

Having established that the simulation of the large-scale part of surface winds depends crucially on the simulation of the large-scale part of the precipitation by the AGCM, we can return briefly to the discussion of the differences in the simulation of the interannual variability by the different AGCMs with similar resolutions (sections 4b,c). As we have chosen the models with comparable resolutions, the differences in the simulations of the surface stress may be related to the differences in the simulation of the precipitation by the different models.

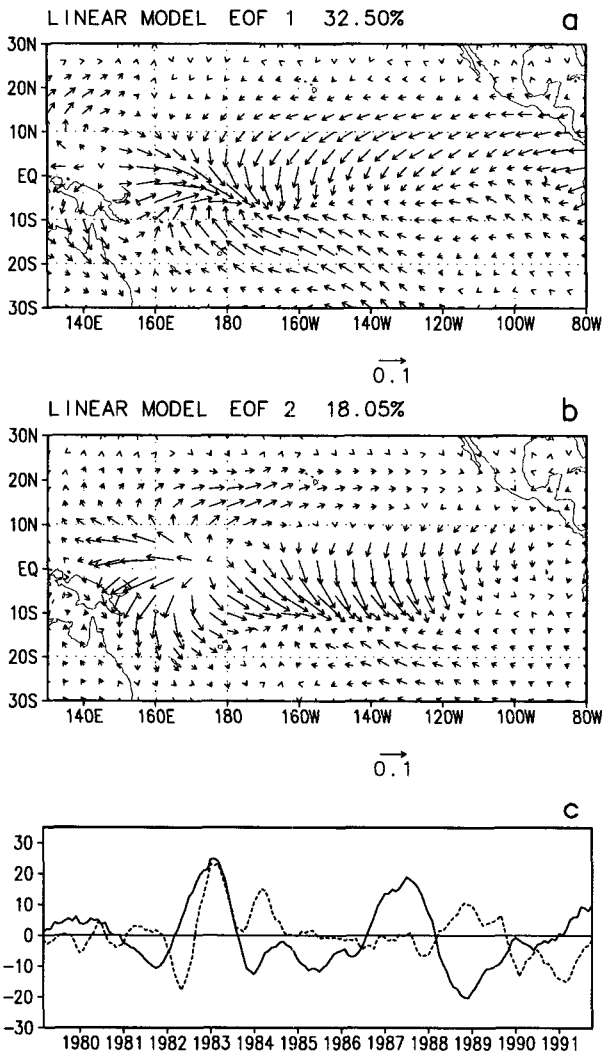


FIG. 16. The first two EOFs and the corresponding PCs of filtered (5-month running mean) zonal winds simulated by a linear Gill-type model forced by the AGCM-simulated precipitation anomalies. The solid line in (c) is PC1 and the dashed line is PC2.

The simulation of the precipitation field, however, depends on parameterization of several physical processes, such as cumulus convection, boundary layer, ground hydrology, and radiation. There are differences in the parameterizations of all these processes in the different models. As a result, it is almost formidable to establish unambiguously the cause of the differences. Part of the success of the COLA model in simulating the large-scale precipitation may be due to its inclusion of the simple biosphere model (Sato et al. 1989).

Our results reinforce the findings in earlier studies (Lau 1985; Latif et al. 1990; Kitoh 1991) and the hypothesis of Charney and Shukla (1981) that the low-frequency component of the tropical variability is forced by slowly varying boundary conditions. In conclusion, one drawback of the present study may be noted. This study is based on only one simulation for 13 years by the GCM. Although the analysis presented here shows that the low-frequency component of the simulated winds is clearly associated with the low-frequency ENSO component of the SST forcing, the high-frequency component of the simulated winds may be partly due to the high-frequency component of the SST forcing and partly due to the internal dynamics of the atmosphere itself. The part of the high-frequency oscillations arising from internal dynamics such as feedback between convection and dynamics is expected to depend sensitively on initial conditions and hence will be unpredictable. In order to isolate the part that would probably be predictable, it will be desirable to conduct a few more experiments with the same boundary conditions but with different initial conditions.

*Acknowledgments.* The authors are thankful to M. Fennessy, J. Kinter, L. Marx, S. Nigam, and J. Shukla for providing the AGCM output, the COADS, and the OLR datasets. They also thank B. Doty for providing the graphics software GrADS, which has been used in many analyses. We also thank L. Gates and P. Gleckler of Lawrence Livermore Laboratory for kindly providing us with some of the AMIP results. B. N. Goswami and N. H. Saji thank the Department of Science and Technology, Government of India, for partial support. V. Krishnamurthy thanks the Jawwaharlal Nehru Centre for Advanced Scientific Research and the Indian

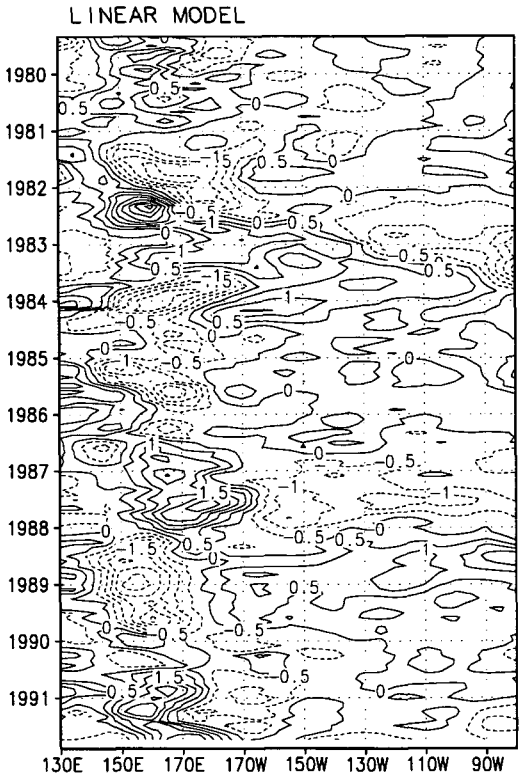


FIG. 17. Filtered (5-month running mean) linear model's simulated zonal winds forced by AGCM precipitation averaged between 6°N and 6°S as a function of time. Contour interval 0.5 m $s^{-1}$.

Institute of Science for hospitality during the course of this work. The authors are also thankful to R. Rama of the Centre for Atmospheric Sciences, Bangalore, Anna Valerio of the Program in Atmospheric and Oceanic Science, Princeton University, New Jersey, for preparing the manuscript, and H. Annamalai for help in analyzing the model output. The authors thank two anonymous reviewers for constructive comments on an earlier version of this manuscript.

## REFERENCES

Battisti, D. S., 1988: Dynamics and thermodynamics of a warming event in a coupled tropical atmosphere–ocean model. *J. Atmos. Sci.*, **45,** 2889–2919.

Charney, J. G., and J. Shukla, 1981: Predictability of monsoon. *Monsoon Dynamics,* J. Lighthill and R. P. Pearce, Eds., Cambridge University Press, 99–109.

Eltahir, E. A. B., and R. L. Bras, 1993: On the response of tropical atmosphere to large scale deforestation. *Quart. J. Roy. Meteor. Soc.*, **119,** 779–793.

Garcia, O., 1985: Atlas of highly reflective clouds for global tropics: 1971–1987. U.S. Department of Commerce, NOAA Environmental Research Laboratory, 365 pp.

Goswami, B. N., and J. Shukla, 1991: Predictability of a coupled ocean–atmosphere model. *J. Climate,* **4,** 3–22.

Graham, N. E., T. P. Barnett, R. M. Chervin, M. E. Schlesinger, and V. Schlese, 1989: Comparison of GCM and observed surface wind fields over the tropical Indian and Pacific Oceans. *J. Atmos. Sci.*, **46,** 760–788.

Kinter, J. L., III, J. Shukla, L. Marx, and E. K. Schneider, 1988: A simulation of winter and summer circulations with the NMC global spectral model. *J. Atmos. Sci.*, **45,** 2486–2522.

Kitoh, A., 1991: Interannual variations in an atmospheric GCM forced by the 1970–1989 SST, Part I: Response of the tropical atmosphere. *J. Meteor. Soc. Japan,* **69,** 251–269.

Kleeman, R., B. J. McAvaney, and R. C. Balgovind, 1994: Analysis of interannual heat flux response in an atmospheric general circulation model of the tropical Pacific. *J. Geophys. Res.*, **99D,** 5539–5550.

Kuo, H. L., 1965: On the formation and intensification of tropical cyclones through latent heat release by cumulus convection. *J. Atmos. Sci.*, **22,** 40–63.

Latif, M., J. Biercamp, H. von Storch, M. McPhaden, and E. Kirk, 1990: Simulation of ENSO related surface wind anomalies with an atmospheric GCM forced by observed SST. *J. Climate,* **3,** 509–521.

——, A. Sterl, El. Maier-Reimer, and M. M. Junge, 1993: Climate variability in a coupled GCM. Part I: The tropical Pacific. *J. Climate,* **6,** 5–21.

Lau, N. C., 1985: Modeling the seasonal dependence of atmospheric response to observed El Niño in 1962–76. *Mon. Wea. Rev.*, **113,** 1970–1996.

——, S. G. H. Philander, and M. J. Nath, 1992: Simulation of ENSO-like phenomena with a low-resolution coupled GCM of the global ocean and atmosphere. *J. Climate,* **5,** 284–307.

Lindzen, R. S., and S. Nigam, 1987: On the role of sea surface temperature gradients in forcing low-level winds in the tropics. *J. Atmos. Sci.*, **44,** 2418–2436.

Mellor, G. L., and T. Yamada, 1982: Development of a turbulence closure model for geophysical fluid processes. *Rev. Geophys. Space Phys.*, **20,** 851–875.

Nagai, T., T. Takioka, M. Endoh, and Y. Kitamura, 1992: El Niño–Southern Oscillation simulated in an MRI atmosphere–ocean coupled general circulation model. *J. Climate,* **5,** 1202–1233.

Neelin, J. D., 1988: A simple model for surface stress and low level flow in the tropical atmosphere driven by prescribed heating. *Quart. J. Roy. Meteor. Soc.*, **114,** 747–770.

——, 1989: On the interpretation of the Gill model. *J. Atmos. Sci.*, **46,** 2466–2468.

——, 1990: A hybrid coupled general circulation model for El Niño studies. *J. Atmos. Sci.*, **47,** 674–693.

——, M. Latif, M. A. F. Allbaart, M. A. Cane, U. Cubasch, W. L. Gate, P. R. Gent, M. Ghil, C. Gordon, N. C. Lau, C. R. Mechoso, G. A. Meehl, J. M. Oberhuber, S. G. H. Philander, P. S. Schopf, K. R. Sperber, A. Sterl, T. Takioka, J. Tribbia, and S. E. Zebiak, 1992: Tropical air–sea interactions in general circulation models. *Climate Dyn.*, **7,** 73–104.

Philander, S. G. H., R. C. Pacanowski, N. C. Lau, and M. J. Nath, 1992: Simulation of ENSO with a global atmospheric GCM coupled to a high-resolution tropical Pacific Ocean GCM. *J. Climate,* **5,** 308–329.

Reynolds, R. W., 1988: A real-time global sea surface temperature analysis. *J. Climate,* **1,** 75–86.

——, and D. C. Marisco, 1993: An improved real-time global sea surface temperature analysis. *J. Climate,* **6,** 114–119.

Sato, N., P. J. Sellers, D. A. Randall, E. K. Schneider, J. Shukla, J. L. Kinter III, Y. T. Hou, and E. Alberyazzi, 1989: Effects of implementing the simple biosphere model in a general circulation model. *J. Atmos. Sci.*, **46,** 2757–2782.

Schopf, P. S., and M. J. Suarez, 1988: Vacillation in a coupled ocean–atmosphere model. *J. Atmos. Sci.*, **45,** 549–566.

Sela, J. G., 1980: Spectral modeling at National Meteorological Center. *Mon. Wea. Rev.*, **108,** 1279–1292.

Sellers, P. J., Y. Mintz, Y. C. Sud, and A. Dalcher, 1986: A simple biosphere model (SiB) for use within general circulation models. *J. Atmos. Sci.*, **43,** 505–531.

Shukla, J., 1981: Dynamical predictability of monthly means. *J. Atmos. Sci.*, **38,** 2547–2572.

Slutz, R. J., S. J. Lubkar, J. D. Hiscox, S. D. Woodruff, R. L. Jenne, D. H. Joseph, P. M. Steurer, and J. D. Elms, 1985: *Comprehensive Ocean–Atmosphere Data Set: Release I.* NOAA Environmental Research Laboratories. Climate Research Program, Boulder, CO, 268 pp.

Tiedke, M., 1984: The effect of penetrative cumulus convection on the large scale flow in a general circulation model. *Beitr. Phys. Atmos.*, **57,** 216–239.

Zebiak, S. E., 1990: Diagnostic study of Pacific surface winds. *J. Climate,* **3,** 1016–1031.

——, and M. A. Cane, 1987: A model El Niño–Southern Oscillation. *Mon. Wea. Rev.*, **115,** 2262–2273.